Supplement of Atmos. Meas. Tech., 8, 4863–4890, 2015
http://www.atmos-meas-tech.net/8/4863/2015/
doi:10.5194/amt-8-4863-2015-supplement

Atmospheric Measurement Techniques
Open Access
EGU

Supplement of

HO_x radical chemistry in oxidation flow reactors with low-pressure mercury lamps systematically examined by modeling

Z. Peng et al.

Correspondence to: J. L. Jimenez (jose.jimenez@colorado.edu)

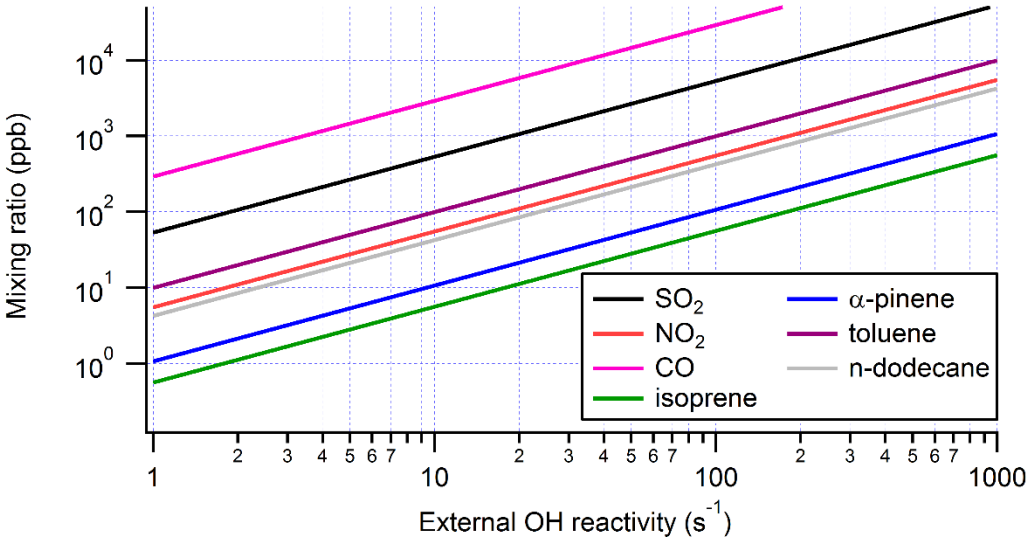

Figure S1. Volume mixing ratios of several external OH reactants corresponding to different external OH reactivities.

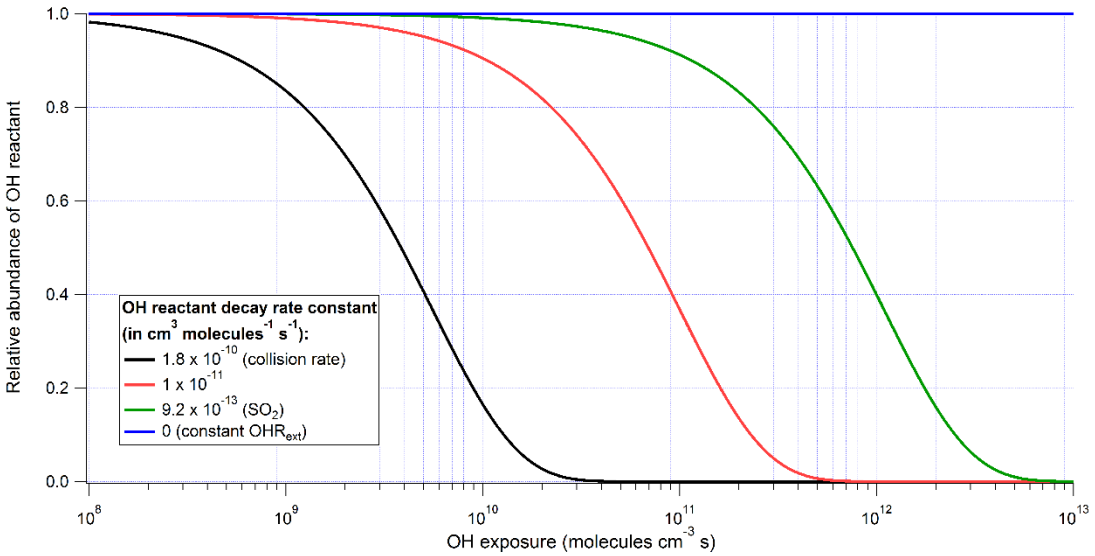

Figure S2. OH reactant abundance relative to the initial value as a function of OH exposure (in molecules cm^{-3} s^{-1}) under the typical condition in Boulder, CO, USA (835 mbar and 295 K). Black, red, green, and blue curves show relative abundance of OH reactant consumed by OH at $1.8x10^{-10}$ (collision rate), $1x10^{-11}$, $9.2x10^{-13}$ (for SO_2 as OH reactant), and 0 (for constant external OH reactivity) cm^3 $molecules^{-1}$ s^{-1}, respectively.

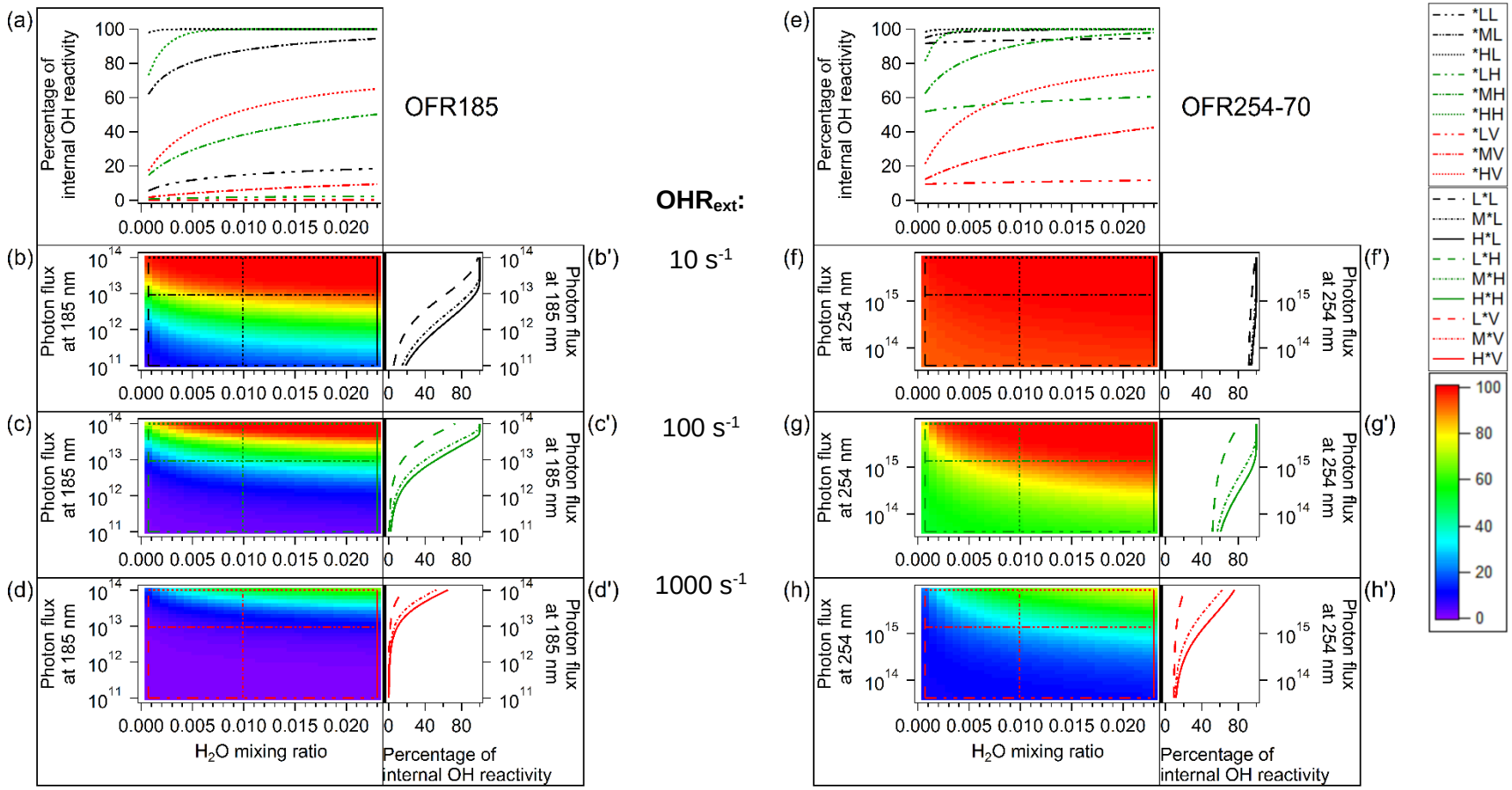

Figure S3. Percentage of internal OH reactivity vs. the same parameters and in the same format as Fig. 2, but without the case of no external OH reactivity, which is the reference case.

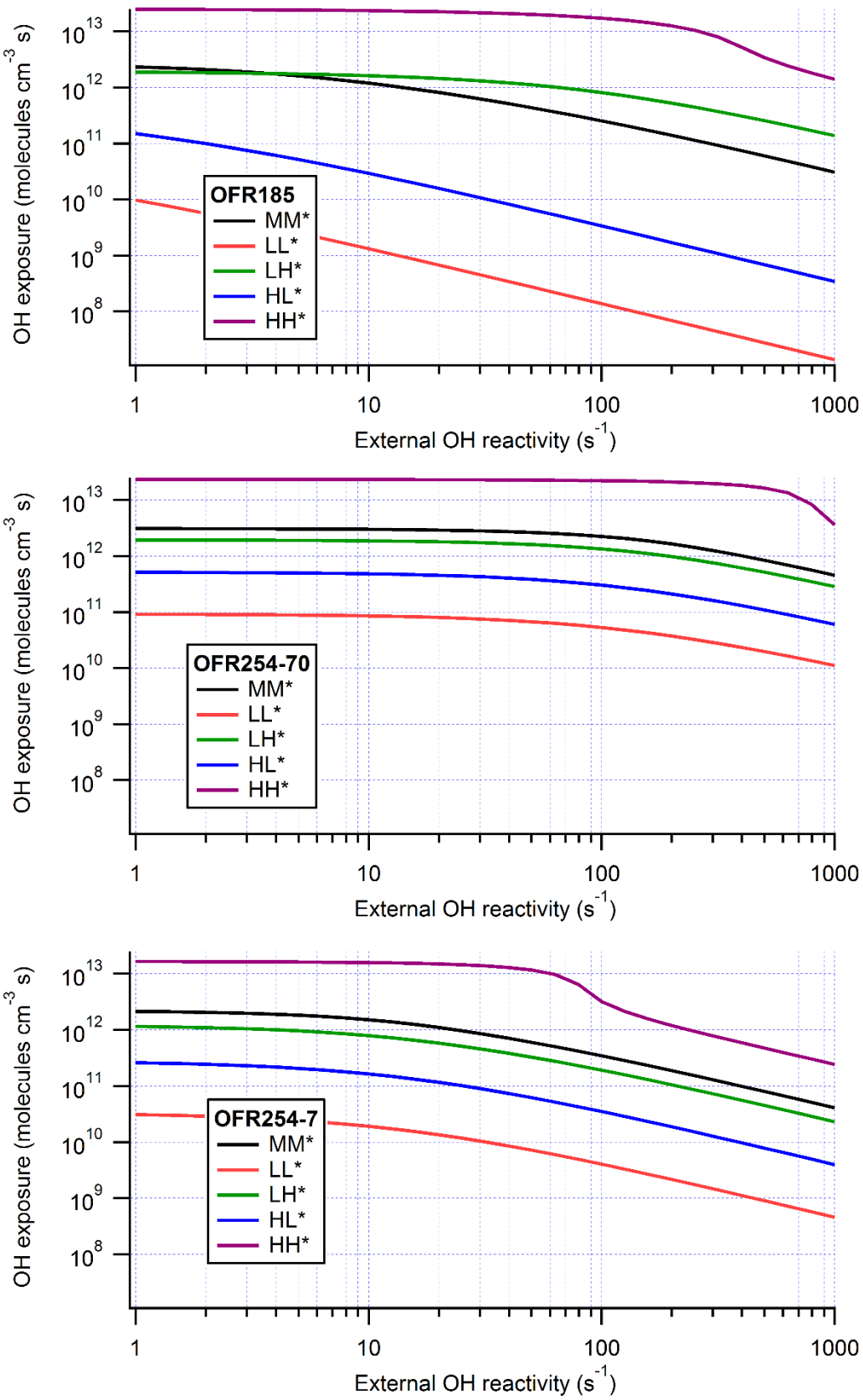

Figure S4. OH exposures in typical cases of OFR185 (top), OFR254-70 (middle), and OFR254-7 (bottom) as a function of external OH reactivity.

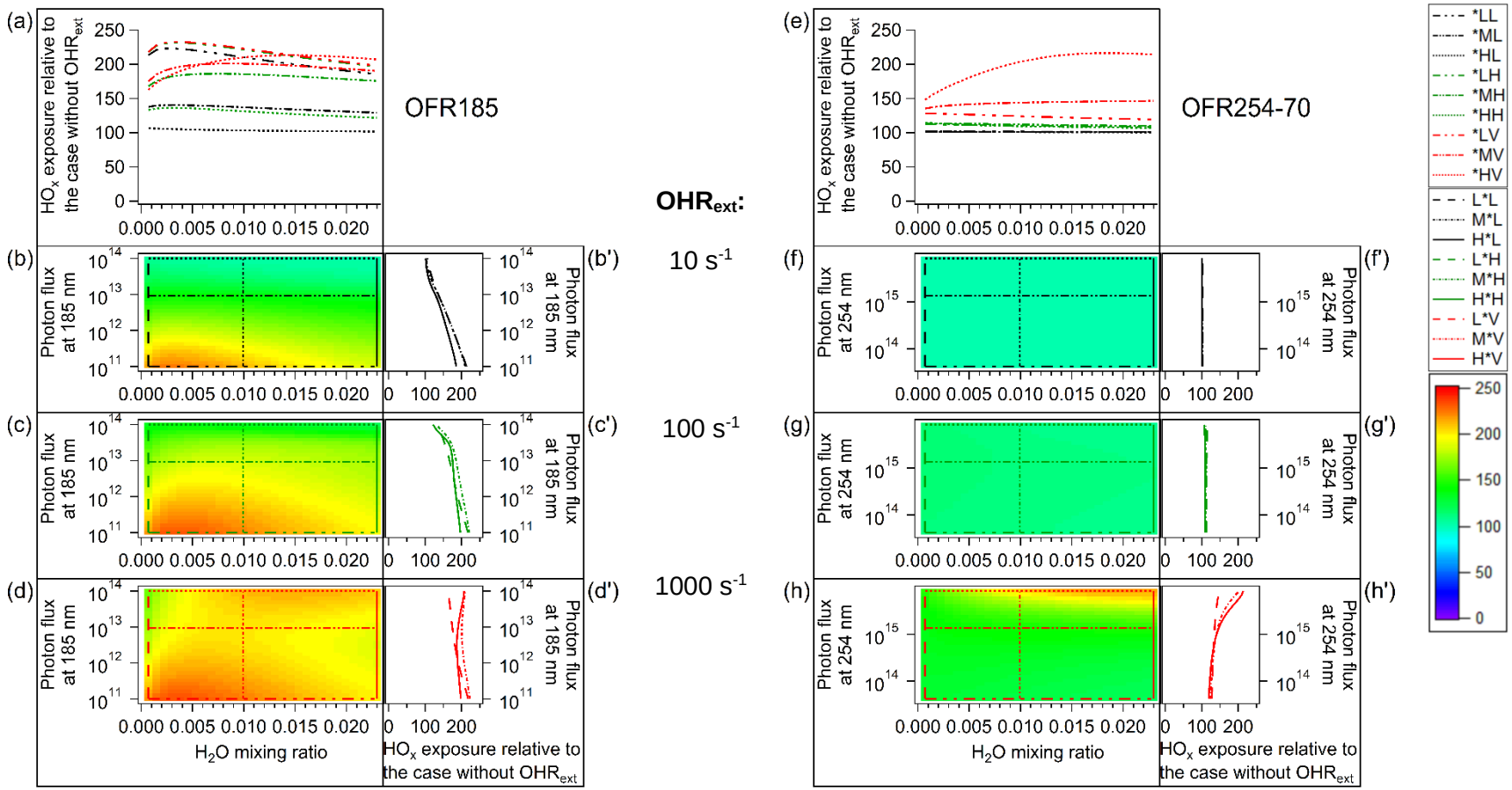

Figure S5. Percentage of total HO_x relative to the case without external OH reactivity (OHR_{ext}) vs. the same parameters and in the same format as Fig. 2, but for the cases of low (10 s^{-1}), high (100 s^{-1}), and very high (1000 s^{-1}) external OH reactivity.

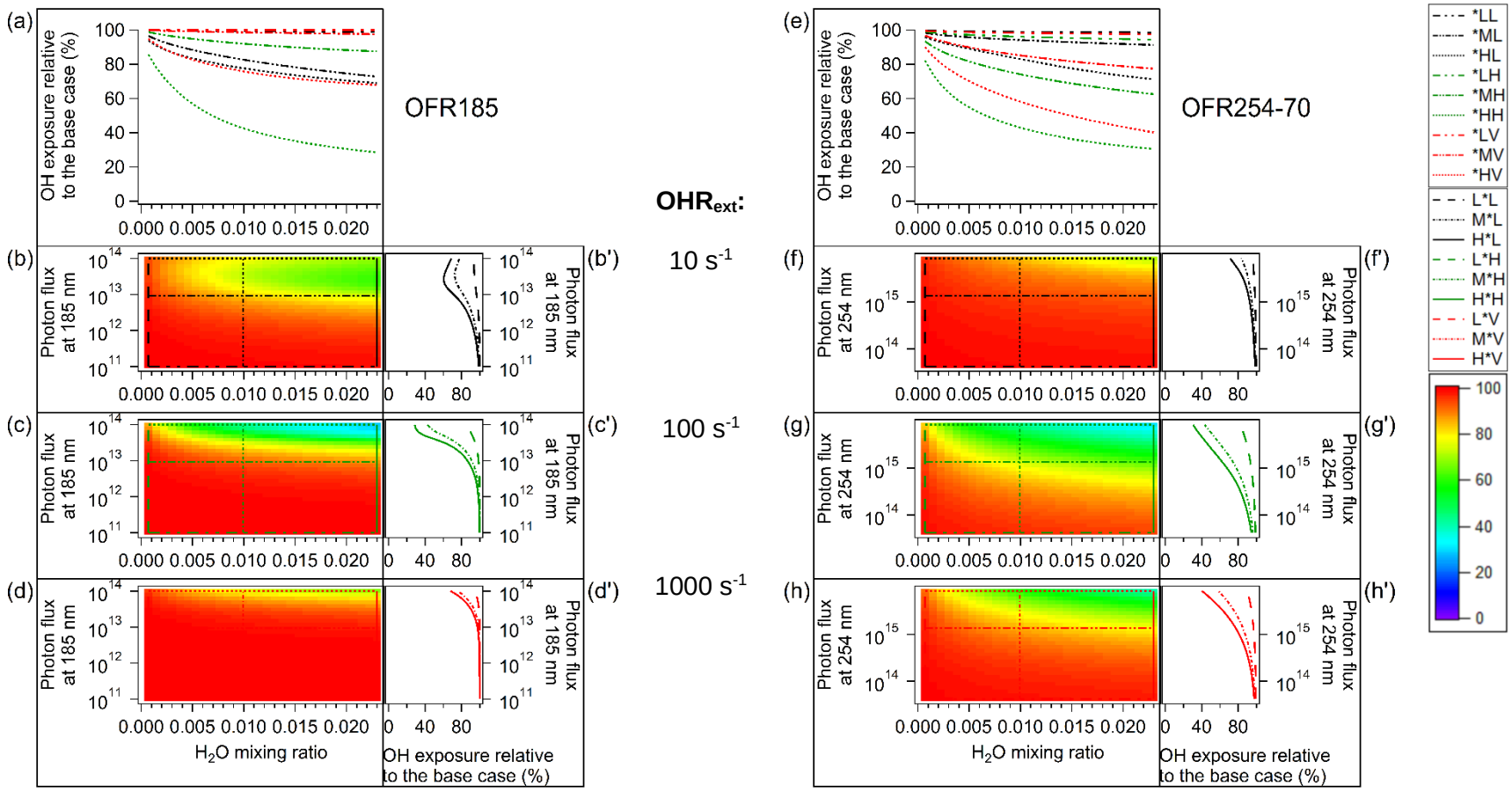

Figure S6. Percentage of OH exposure in the case of constant external OH reactivity (OHR_{ext}) relative to that in the base case (Fig. 2) vs. the same parameters and in the same format as Fig. S3.

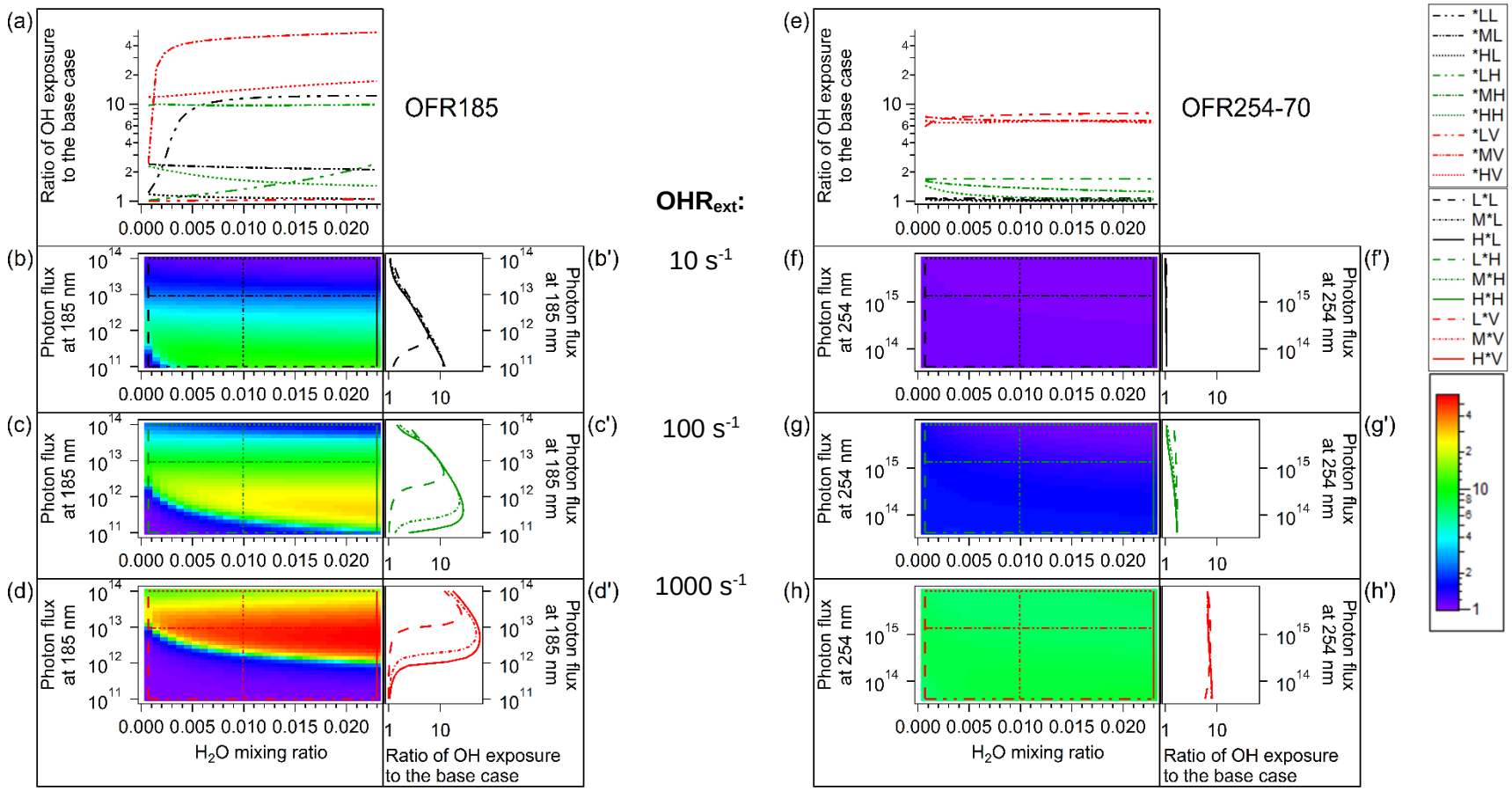

Figure S7. Ratio of OH exposure in the case of external OH reactivity (OHR_{ext}) decaying at collision rate to that in the base case (Fig. 2) vs. the same parameters and in the same format as Fig. S3.

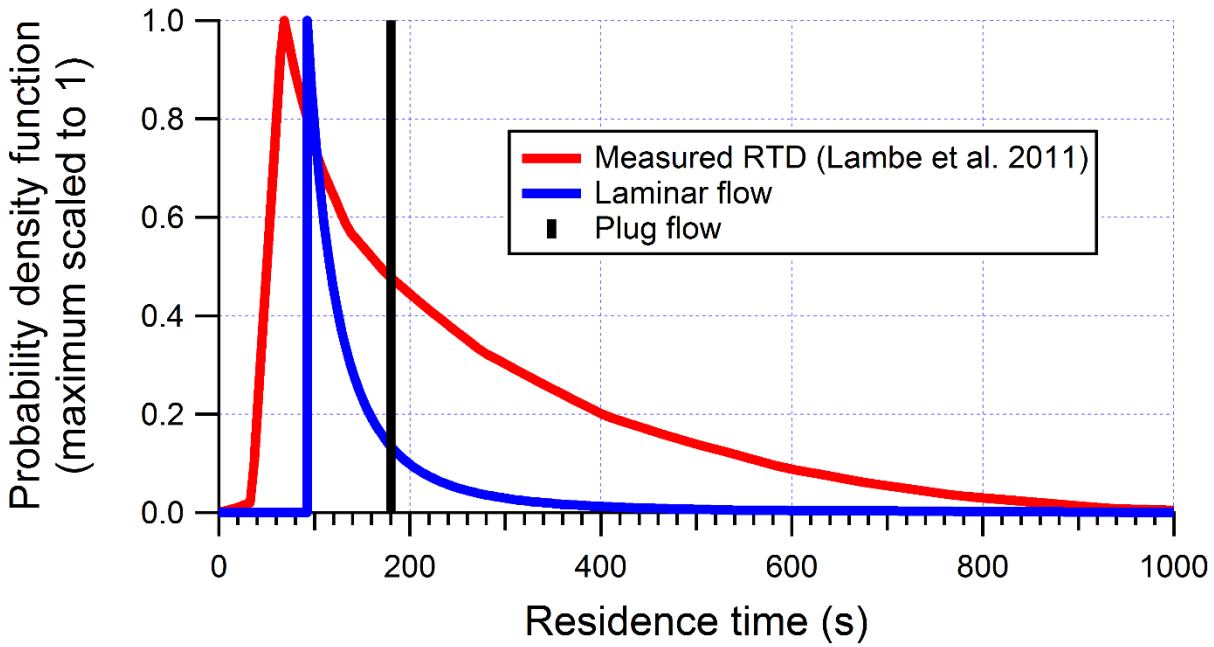

Figure S8. Residence time distribution (RTD) of plug and flows with the (average) residence time of 180 s and measured residence time distribution for the PAM (Lambe et al., 2011), linearly scaled for the average residence time to be 180 s.

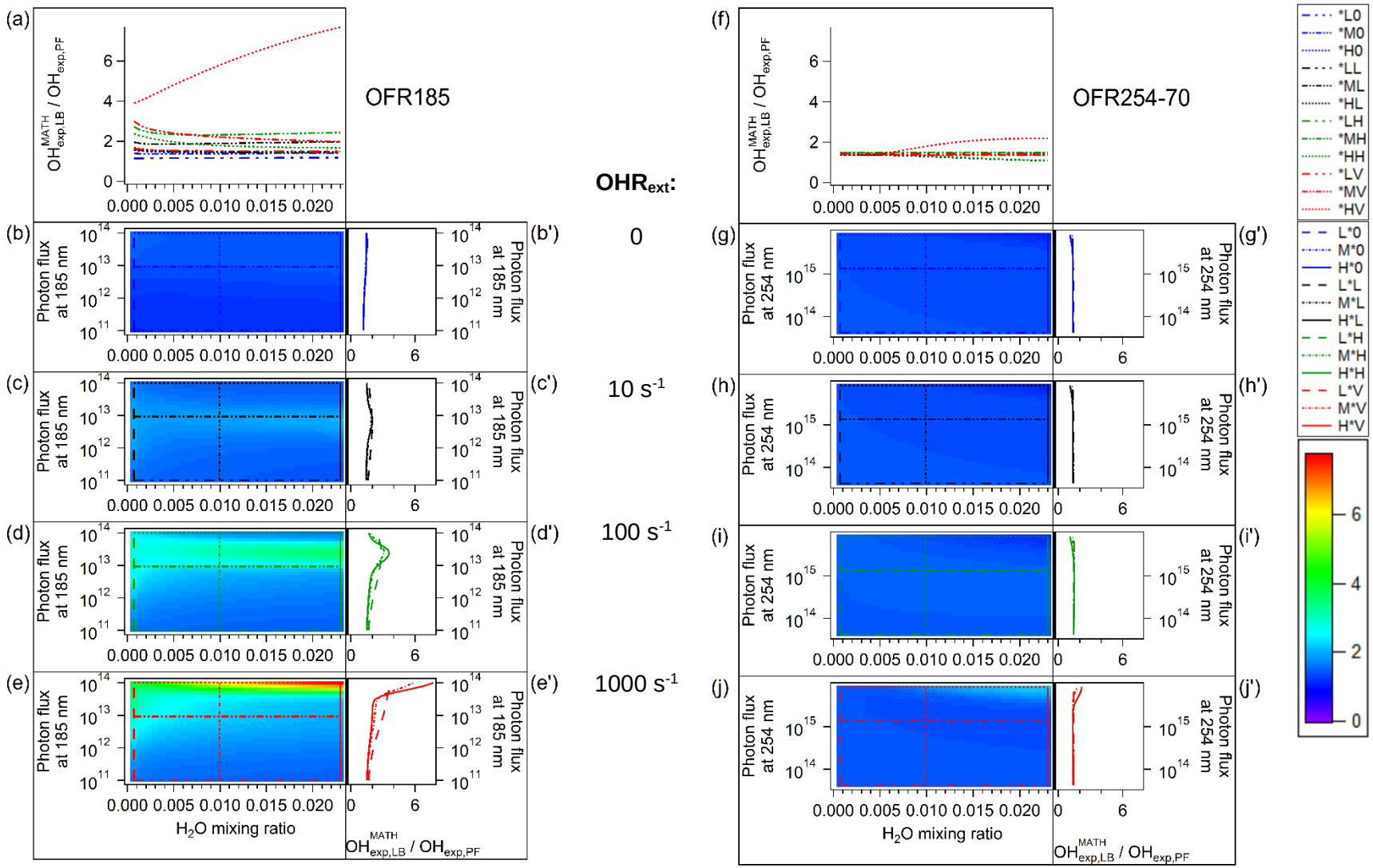
(a)
OFR185
(f)
OFR254-70
OHR_ext:
0
10 s-1
100 s-1
1000 s-1
(b)
(b')
(c)
(c')
(d)
(d')
(e)
(e')
(g)
(g')
(h)
(h')
(i)
(i')
(j)
(j')
Photon flux at 185 nm
Photon flux at 254 nm
H2O mixing ratio
OH_exp,LB^MATH / OH_exp,PF
*L0
*M0
*H0
*LL
*ML
*HL
*LH
*MH
*HH
*LV
*MV
*HV
L*0
M*0
H*0
L*L
M*L
H*L
L*H
M*H
H*H
L*V
M*V
H*V

Figure S9. Dependence of the ratios of OH exposure calculated from direct integration in the model with measured residence time distribution (Lambe et al., 2011) ($OH_{exp,RTD}^{MATH}$) to that in the plug-flow model ($OH_{exp,PF}$) vs. the same parameters and in the same format Fig. 2.

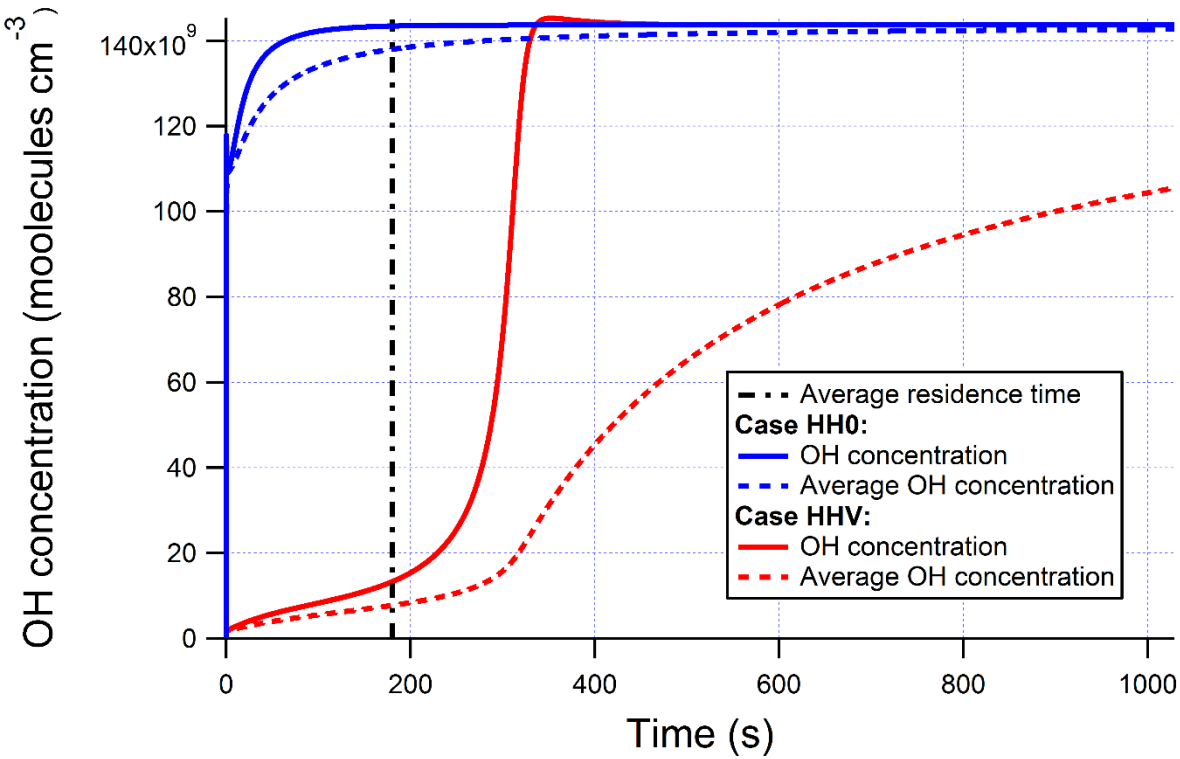

Figure S10. Instantaneous OH concentration vs. residence time in the reactor for Cases HH0 (OHR_{ext} = 0) and HHV (OHR_{ext} = 1000 s^{-1}) in OFR185. For each case, average OH concentration over the elapsed reaction time is also shown. All curves (both instantaneous and integrated averages) are for individual air parcels and thus independent of model flow distributions.

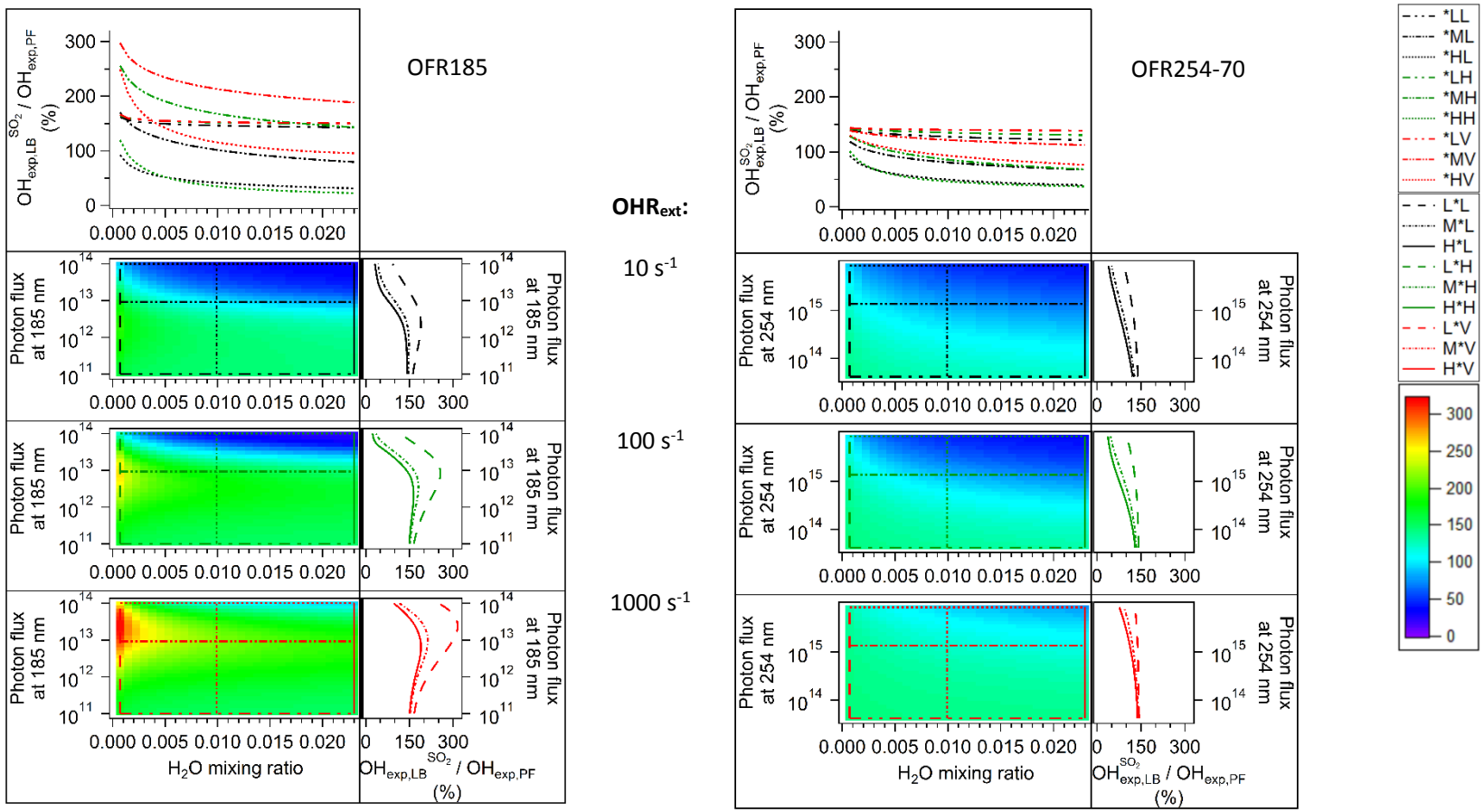

Figure S11. Percentage of OH exposure estimated from SO_2 decay in the model with the Lambe et al. (2011a) residence time distribution ($OH_{exp,LB}^{SO_2}$) to OH exposure in the plug-flow model ($OH_{exp,PF}$) vs. the same parameters and in the same format as Fig. 5.

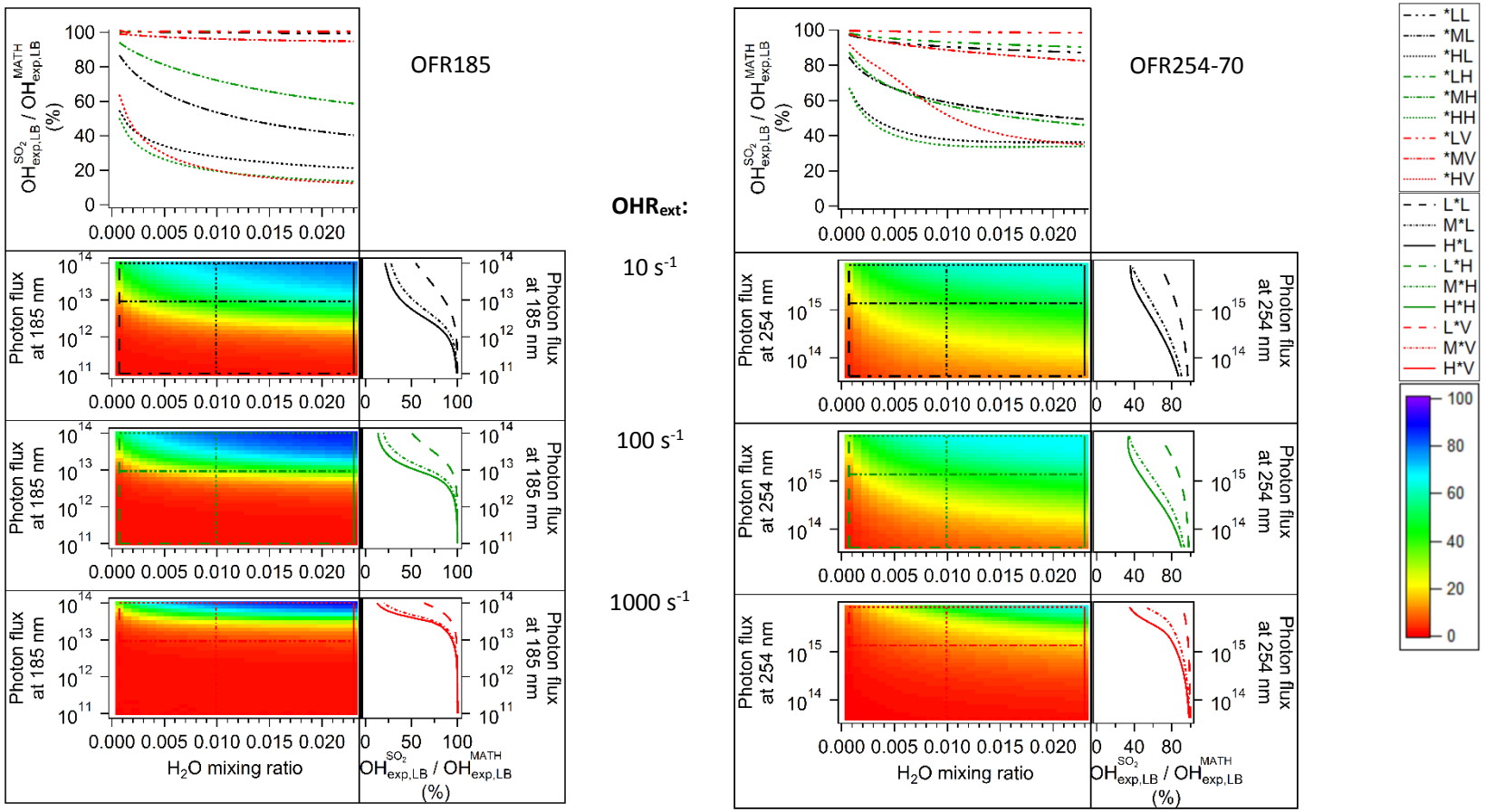

Figure S12. Percentage of OH exposure estimated from SO_2 decay in the model with the Lambe et al. (2011a) residence time distribution ($OH_{exp,LB}^{SO_2}$) to that calculated from direct integration in the same model ($OH_{exp,LB}^{MATH}$) vs. the same parameters and in the same format as Fig. 5.

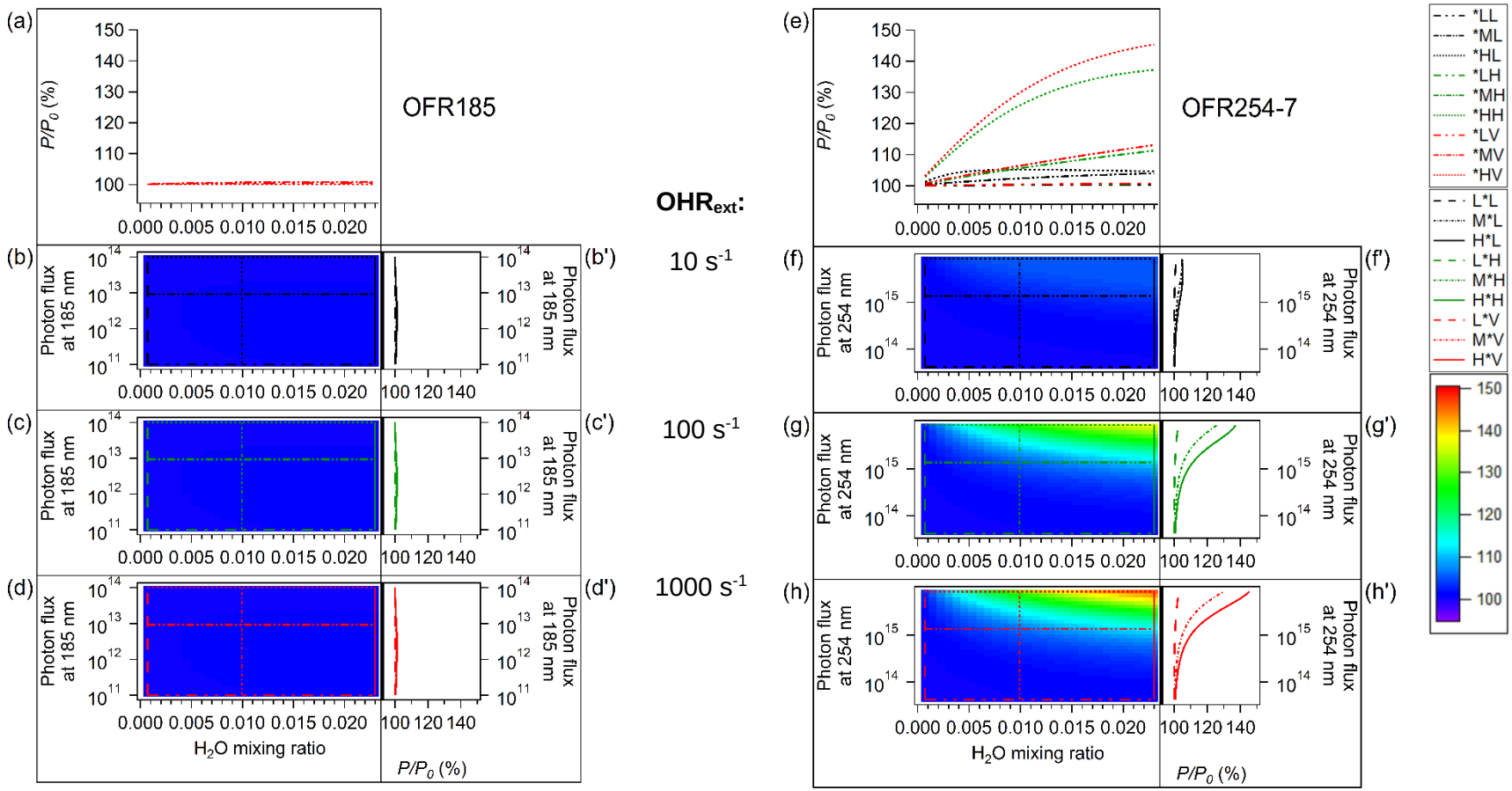

Figure S13. Percentage of OH production rate to that at the same H_2O and UV but OHR_{ext}=0 vs. the same parameters and in the same format as Fig. 5.

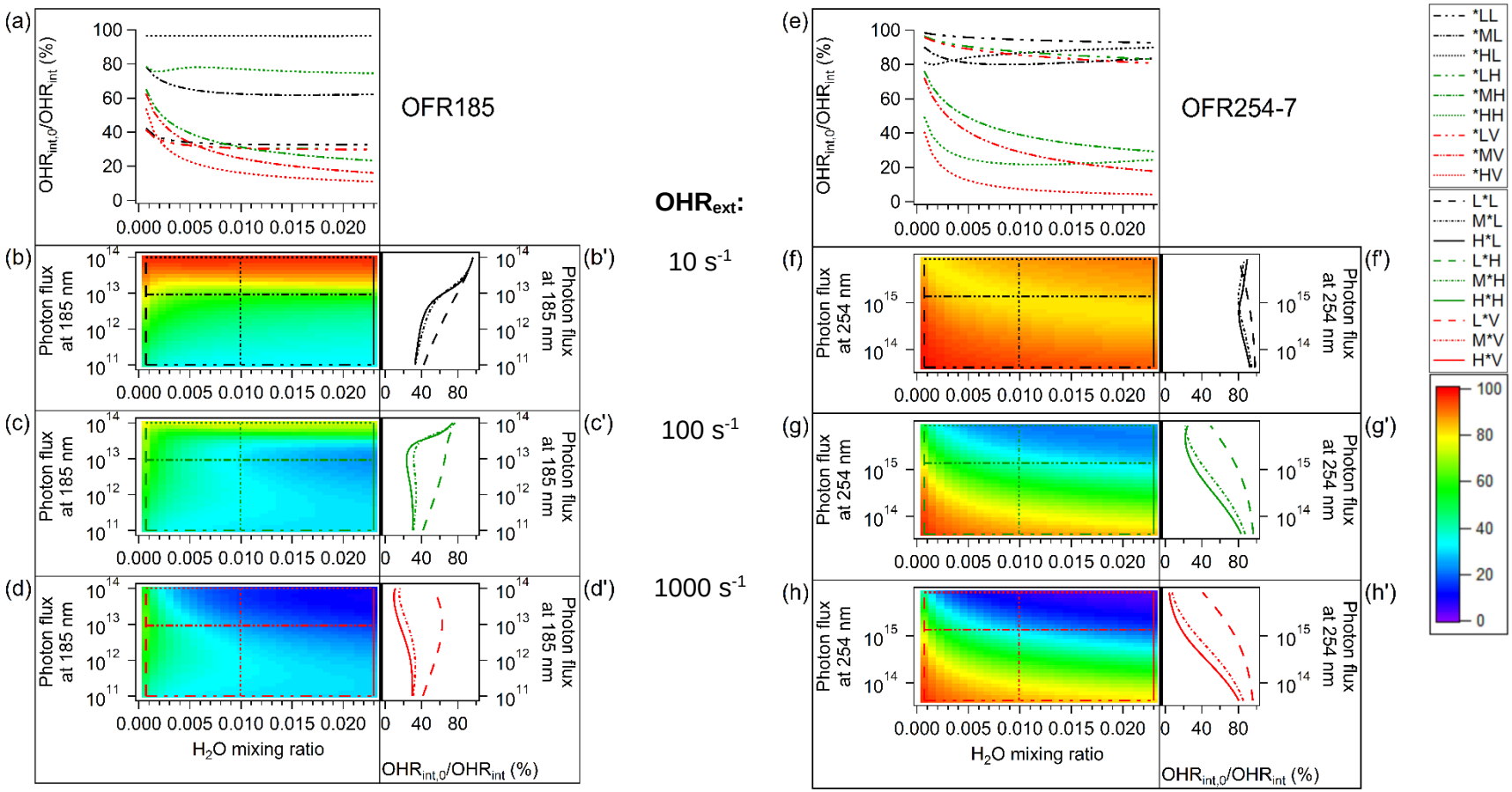

Figure S14. Percentage of OHR_{int} to that at the same H_2O and UV but OHR_{ext}=0 vs. the same parameters and in the same format as Fig. 5.

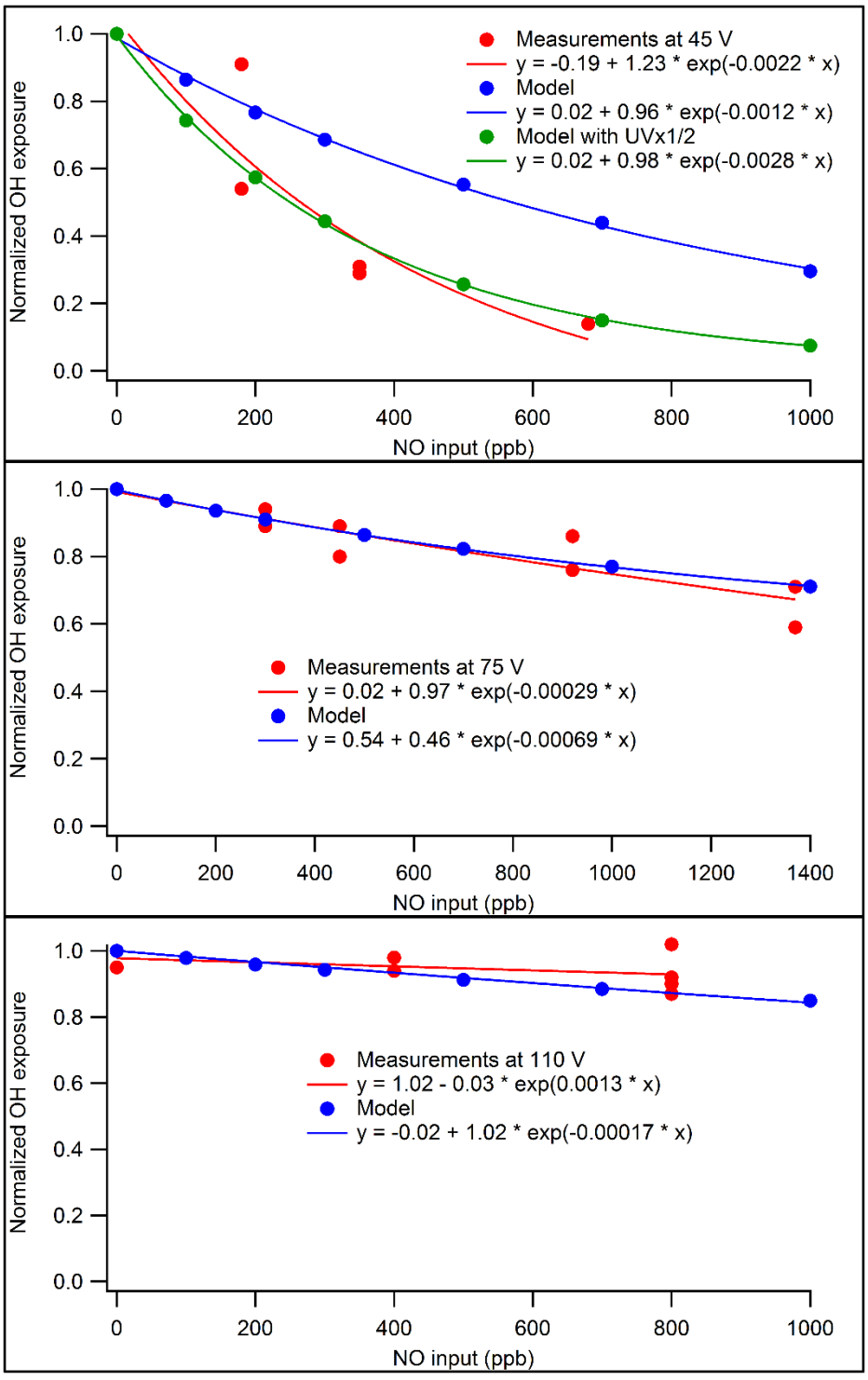

Figure S15. Modeled (blue with full UV and green with half UV) and measured (red; Tkacik et al., 2014) OH exposures in the PAM normalized to that in the case without NO as a function of initial NO input (in ppb) at the lamp voltages of 45 (top), 75 (middle), and 110 V (bottom). Exponential fitting curves for the measurements reported in Tkacik et al. (2014) and the model predictions in this study are also shown.

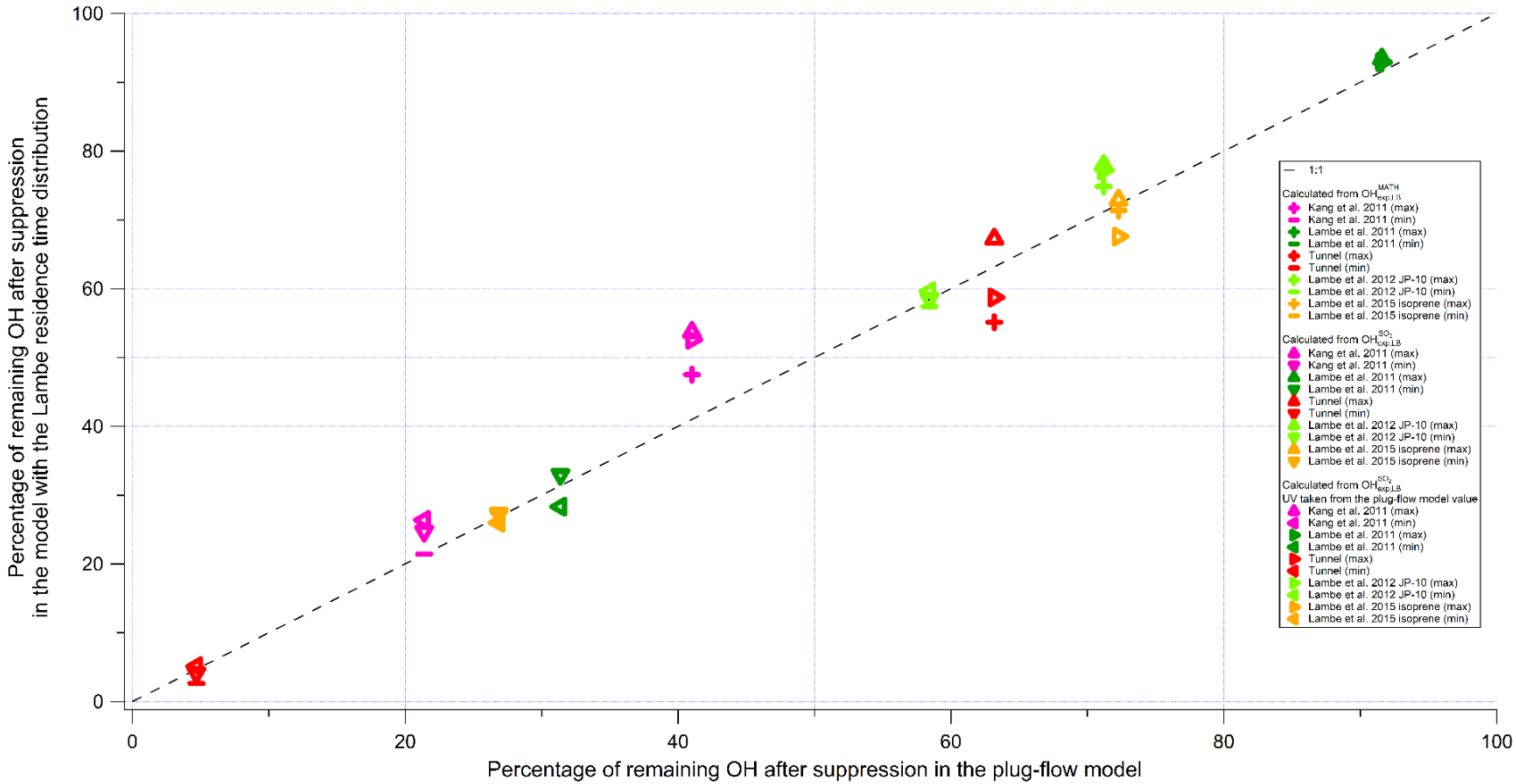

Figure S16. Percentage of remaining OH after suppression in the model with the Lambe et al. (2011a) residence time distribution vs. that in the plug-flow model. The former is calculated from i) directly integrated OH exposure ($OH_{exp,LB}^{MATH}$), ii) OH exposure estimated from SO_2 (as a tracer in most literature experiments) decay ($OH_{exp,LB}^{SO_2}$), and iii) $OH_{exp,LB}^{SO_2}$ obtained with UV estimated in the plug-flow model.

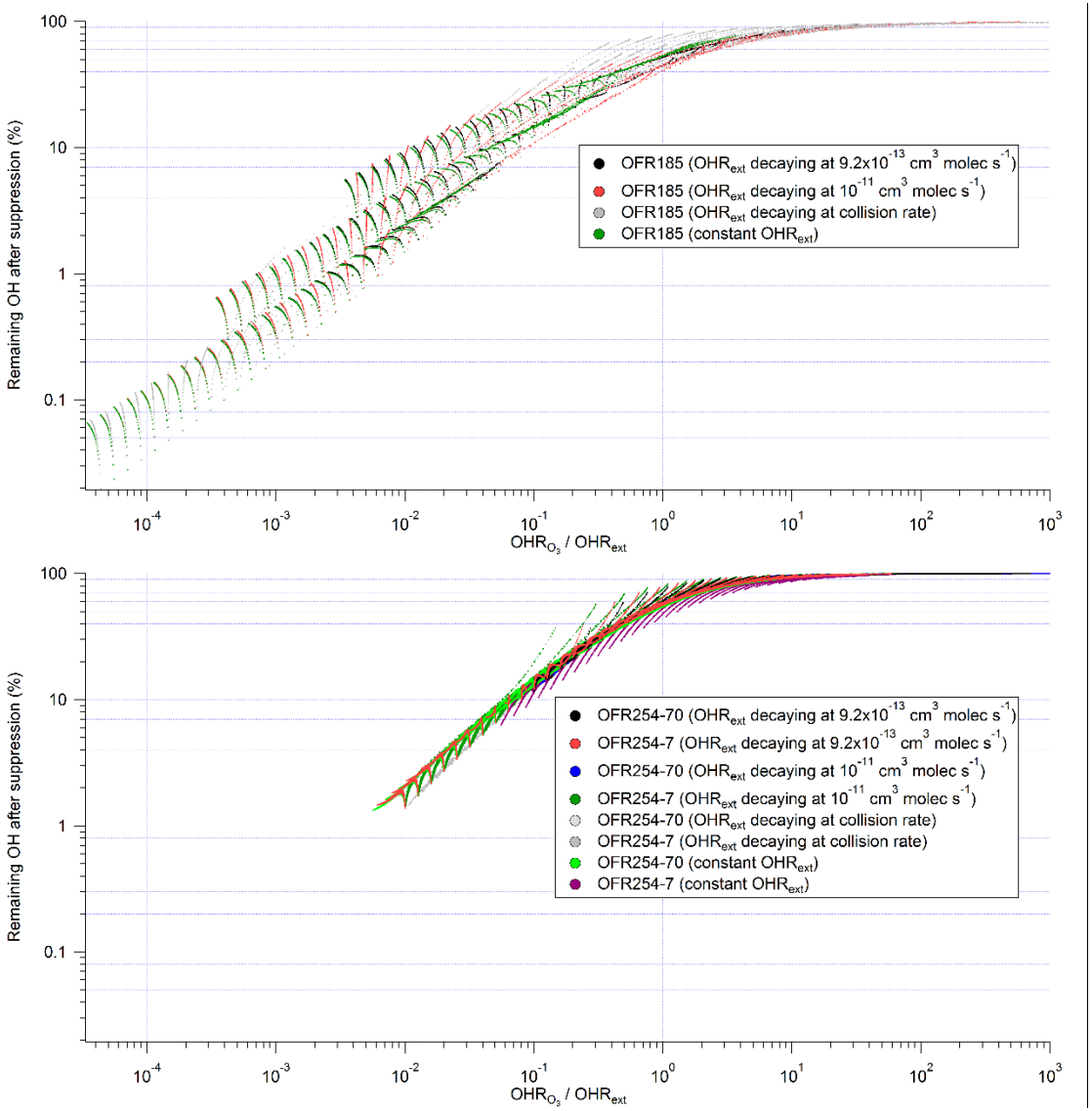

Figure S17. Percentage of remaining OH after suppression in OFR185 (upper) and OFR254 (lower) in the same format as Fig. 8. Within each plot, cases with OHR_{ext} decaying at $1x10^{-11}$ cm^3 $molecules^{-1}$ s^{-1} and collision rate and constant OHR_{ext} are contrasted with the base case (SO_2 as OH reactant, decaying at $9.2x10^{-13}$ cm^3 $molecules^{-1}$ s^{-1}).

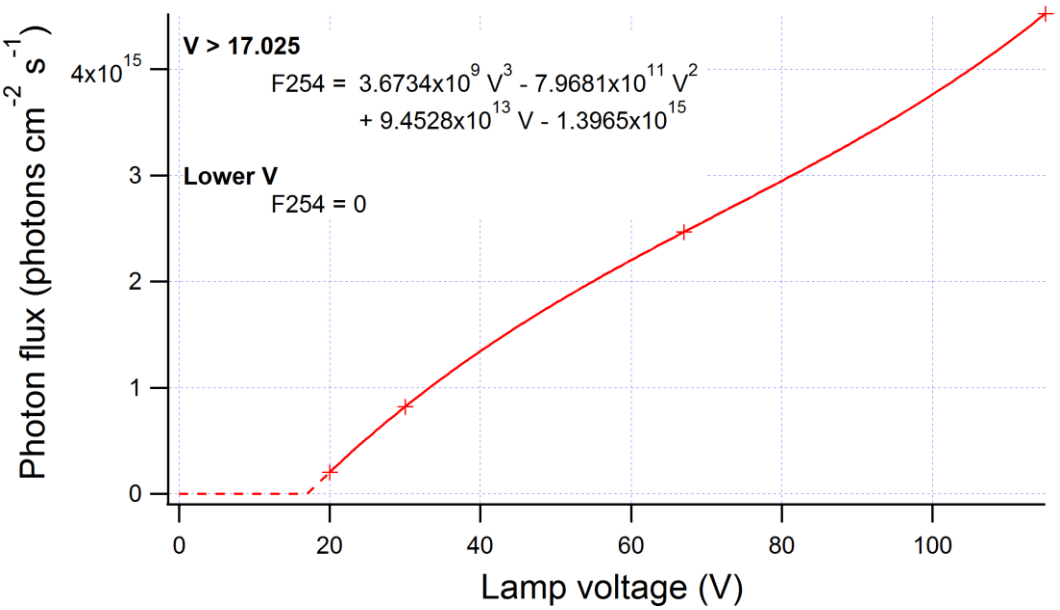

Figure S18. Low-pressure Hg lamp emission at 254 nm as a function of lamp voltage. The markers show data points from Li et al. (2015)'s estimation. The curve is obtained by fitting the data points with a 4-parameter polynomial. Voltages lower than 17.025 V (the curve's intercept with the abscissa) result in no photon emission.

Table S1. Statistics of the ratio among OH exposures calculated in the models with the laminar and Lambe et al. (2011a) residence time distributions ($OH_{exp,RTD}^{MATH}$), estimated from SO_2 decay in the same model ($OH_{exp,RTD}^{SO_2}$), and calculated in the plug-flow model ($OH_{exp,PF}$). The geometric mean, uncertainty factor, and percentage of outlier cases (>2 or <1/2) are shown for OFR185, OFR254-70, and OFR254-7. Statistics for all cases with the laminar and Lambe et al. residence time distributions are also reported.

OFR type	$OH_{exp,RTD}^{MATH}$ / $OH_{exp,PF}$			$OH_{exp,RTD}^{SO_2}$ / $OH_{exp,PF}$			$OH_{exp,RTD}^{SO_2}$ / $OH_{exp,RTD}^{MATH}$		
	Geom. Mean	Uncert. factor	Outlier cases (%)	Geom. mean	Uncert. factor	Outlier cases (%)	Geom. mean	Uncert. factor	Outlier cases (%)
OFR185 Laminar	0.86	1.06	0	0.79	1.19	2	0.90	1.19	2
OFR185 Lambe	1.75	1.35	23	1.35	1.58	13	0.70	1.67	22
OFR254-70 Laminar	0.86	1.02	0	0.76	1.11	0	0.89	1.11	0
OFR254-70 Lambe	1.42	1.09	0	0.95	1.40	6	0.67	1.39	21
OFR254-7 Laminar	0.86	1.02	0	0.81	1.10	0	0.94	1.10	0
OFR254-7 Lambe	1.41	1.10	0	1.12	1.34	2	0.80	1.34	12
All Cases Laminar	0.86	1.04	0	0.79	1.14	1	0.91	1.14	1
All Cases Lambe	1.52	1.24	8	1.13	1.49	7	0.72	1.49	15

Table S2. Fitting parameters of the two estimation equations (Eqs. 11 and 12).

Eq. 11				Eq. 12	
a	15.514	c_2	0.060786	a	13.322
b_1	0.79292	d	-0.42602	b	-0.22101
b_2	0.023076	e	0.39479	c	0.43529
c_1	-1.0238				

Reference

Lambe, A. T., Ahern, A. T., Williams, L. R., Slowik, J. G., Wong, J. P. S., Abbatt, J. P. D., Brune, W. H., Ng, N. L., Wright, J. P., Croasdale, D. R., Worsnop, D. R., Davidovits, P. and Onasch, T. B.: Characterization of aerosol photooxidation flow reactors: heterogeneous oxidation, secondary organic aerosol formation and cloud condensation nuclei activity measurements, Atmos. Meas. Tech., 4(3), 445–461, doi:10.5194/amt-4-445-2011, 2011.

Li, R., Palm, B. B., Ortega, A. M., Hu, W., Peng, Z., Day, D. A., Knote, C., Brune, W. H., de Gouw, J. and Jimenez, J. L.: Modeling the radical chemistry in an Oxidation Flow Reactor (OFR): radical formation and recycling, sensitivities, and OH exposure estimation equation, J. Phys. Chem. A, 119(19), 4418–4432, doi:10.1021/jp509534k, 2015.

Tkacik, D. S., Lambe, A. T., Jathar, S., Li, X., Presto, A. A., Zhao, Y., Blake, D., Meinardi, S., Jayne, J. T., Croteau, P. L. and Robinson, A. L.: Secondary Organic Aerosol Formation from in-Use Motor Vehicle Emissions Using a Potential Aerosol Mass Reactor., Environ. Sci. Technol., 48(19), 11235–42, doi:10.1021/es502239v, 2014.